A Wearable and Wirelessly Powered System for Multiple Finger Tracking

Paolo Bellitti, Alessio De Angelis, *Member, IEEE*, Marco Dionigi, Emilio Sardini, Mauro Serpelloni, Antonio Moschitta, *Member, IEEE*, and Paolo Carbone, *Fellow, IEEE*

***Abstract*— A wearable system that is capable of tracking finger motion and recognizing a set of hand gestures is presented. Two tracking units are worn on two fingers and are wirelessly powered without using cables or batteries, thus enhancing freedom of movement. The system is comprised of two sections: a measurement section and a wireless power transfer apparatus. The measurement section consists of two measuring devices placed on the thumb and index fingers. Each of these units can acquire and transmit sensor signals obtained from a stretch sensor and an inertial measurement unit. Furthermore, the wireless power transfer apparatus is implemented by means of inductively coupled resonant circuits. A relay-resonator configuration is employed to provide a homogeneous magnetic field in the operating volume of the system. A prototype of the developed system is characterized by experimental tests. Results show that the proposed approach is feasible. The measuring system can track finger movement with a sample rate of 30 Hz and recognize six predefined gestures used to control a robotic arm. The wireless power transfer apparatus demonstrates the capability of transferring 110 mW, necessary to power the measurement section, within an operating volume of 25 cm × 20 cm × 15 cm.**

***Index Terms*— Finger tracking, gesture recognition, stretch sensor, wireless power transfer.**

I. Introduction

MOTION tracking of a human subject's hands and fingers is a crucial feature of several industrial and biomedical applications. Specifically, it is required for implementing human–machine interfaces (HMIs), such as the finger position sensing system described in [1]. Furthermore, it allows for the development of human-robot cooperation, such as the methods presented in [2]. In the biomedical field, motion tracking is applied for monitoring specific hand rehabilitation exercises, as described in [3]. Several technologies have been proposed for the purpose of tracking hand and finger motion, including camera-based optical systems [4], magnetic-field localization solutions [5], and inertial measurement units (IMUs) [6].

Manuscript received August 8, 2019; revised December 17, 2019; accepted January 3, 2020. Date of publication October 23, 2019; date of current version April 7, 2020. This work was supported by the Italian Ministry of Instruction, University and Research under Grant PRIN 2015C37B25. The Associate Editor coordinating the review process was Vedran Bilas. *(Corresponding author: Alessio De Angelis.)*

Paolo Bellitti, Emilio Sardini, and Mauro Serpelloni are with the Department of Information Engineering, University of Brescia, 25121 Brescia, Italy.

Alessio De Angelis, Marco Dionigi, Antonio Moschitta, and Paolo Carbone are with the Department of Engineering, University of Perugia, 06125 Perugia, Italy (e-mail: alessio.deangelis@unipg.it).

Color versions of one or more of the figures in this article are available online at http://ieeexplore.ieee.org.

Digital Object Identifier 10.1109/TIM.2020.2969089

Furthermore, hand motion tracking enables gesture recognition, which is a practical and ergonomic way to issue commands to an electronic device or a smart environment [7]. There are numerous contexts in which it is more convenient than a conventional HMI, such as a keyboard, mouse, or any other physical input peripheral. First, these input peripherals are typically comprised of buttons and switches that are subject to mechanical failures. Thus, replacing them with noncontact interfaces, based on motion tracking, improve reliability and durability [8]. Moreover, in an industrial environment, an operator can be unable to use the control panel of a specific machine. Therefore, sending commands from a distance in a wireless and natural way can be convenient. For example, a telemanipulator [9], [10] could be actuated by mimicking hand and fingers' positions, or a collaborative robot could be programed to start a specific routine in an assembly line.

In the literature, several studies address the problem of optical hand gesture recognition. An example based on data acquired by two cameras and processed by fuzzy neural networks is provided in [7]. Furthermore, [11] and [12] give an overview of currently employed methods. These methods use cameras and illuminators, in association with image processing algorithms, to estimate the hand position [13]. With this approach, high-performance levels can be reached, but it is critical to maintaining the line of sight with the cameras. Furthermore, the overlap of two tracked objects can increase uncertainty [14]. Finally, these methods typically maintain performance only in controlled illumination conditions. In some environments, such as the industrial one, these disadvantages can be accentuated enough to make their use unsuitable. For these reasons, in this article, we focus on a nonoptical approach.

Among the nonoptical technologies, short-range magnetic tracking systems, which employ artificially generated ac magnetic fields, have been proposed in the literature. Using these systems, finger movements can be tracked with accuracy on the order of 3 mm, without requiring line-of-sight [15]. This is an advantage with respect to optical solutions. Nevertheless, magnetic tracking systems are affected by field disturbances due to ferromagnetic and conductive materials in the environment [16].

On the other hand, systems based on data gloves are heavily used both in industrial and commercial contexts [17]. These systems are composed of a wearable device, usually equipped with inertial modules and stretch sensors applied near the

interphalangeal joints [18]–[20]. Data gloves-based systems permit to collect more reliable data than optical systems [21]. However, they can result in physical constraints for some movements, due to the presence of wires used for signaling and powering purposes. Conversely, wireless solutions avoid such constraints. To transfer data, protocols for personal area networking, such as Bluetooth low energy (BLE), are commonly employed. Besides, to transfer power, wireless power transfer (WPT) systems are widely investigated in the literature for portable electronics, biomedical applications, and electric vehicles [22]. In particular, the inductive coupling of resonators is the preferred technology for developing medium-range WPT links [23], [24]. A measurement methodology for characterizing WPT systems in terms of the amount of power delivered to the load and the efficiency is presented in [25].

The measuring system proposed in this article is wearable, powered by a WPT apparatus within an operating volume of 25 cm × 20 cm × 15 cm, and able to track the hand motion by means of stretch sensors and IMUs. The measuring device is integrated into small modules that can be worn on each finger autonomously. According to every specific need and usage case, the minimum number of modules can be used to reduce physical constraints. As an example, to control a pointer on a screen, it is enough to track a single finger with one module. Preliminary results on the development of a single-finger tracking system were presented in [26].

For gesture recognition applications, or to manipulate physical or virtual objects, multiple modules can be worn on different fingers. In this article, we present a gesture recognition method based on tracking two fingers, which is experimentally evaluated using the realized measuring system prototype. The main feature of the proposed system is that power supply and data transfer are provided wirelessly. This feature allows utilizing the stretch sensors and IMUs for accurate finger tracking without cables or constraints. Compared with the widely used optical systems from the literature, the proposed system is robust to obstructions of the line of sight and varying levels of illumination. Furthermore, compared with preexisting data glove solutions, the advantage of the proposed system is that it does not require cables. Therefore, user motion constraints are avoided and usability improves.

II. Architecture of the Proposed System

The architecture of the proposed system (illustrated in Fig. 1) is composed of two main subsystems. The first subsystem is represented by a wearable measurement device that can be worn on a single finger. The modular approach permits to wear one or multiple independent measurement devices based on the number of fingers whose movements are to be tracked. In comparison with current data glove-based systems, which are intrinsically nonmodular [17]–[19], this is an improvement since it reduces the physical constraints, especially in those cases where monitoring of all five fingers is not required. Moreover, the measurement device module does not require wiring since it exploits wireless connection for data transfer and wireless power transfer for power supply. A single-measuring device module, excluding the plastic fixing ring and considering only the electronics in its enclosure, has

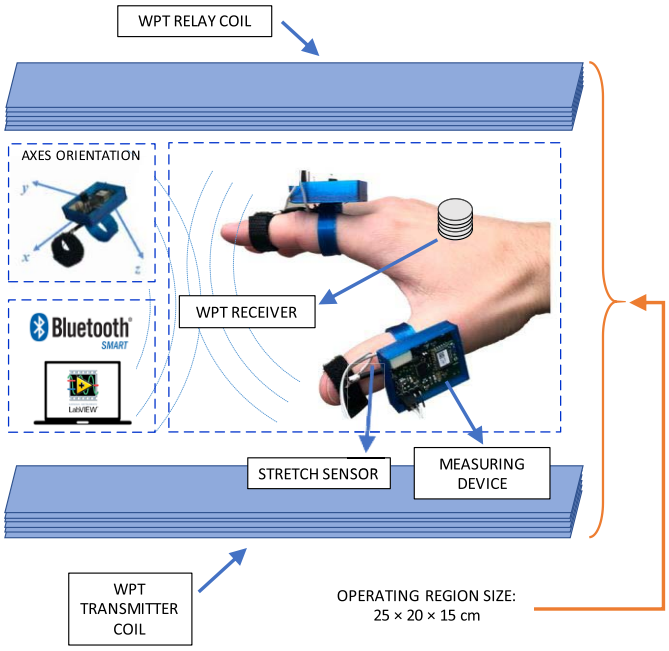

Fig. 1. Architecture of the proposed system. Two measuring devices with stretch sensors are worn on two fingers and powered by a wireless power transfer subsystem. Each measuring device tracks one finger independently. The size of the region of space in which the tracking system is operational and able to be powered wirelessly by the WPT subsystem is 25 cm × 20 cm × 15 cm. The size of the measuring device worn on the finger is 37 mm × 27 mm × 10 mm.

dimensions of 37 mm × 27 mm × 10 mm and a weight of 9.6 g. The weight does not include batteries since the device is not equipped with them, being powered by the wireless power transfer subsystem.

The custom-developed electronic board of each measurement device is equipped with all the peripherals and sensors needed to carry out the measurement operation and to transmit the retrieved data wirelessly. Moreover, a readout unit receives and interprets the finger movements. In our implementation, the readout unit is composed by a personal computer with a BLE module and LabVIEW virtual instrument program.

The second part of the architecture is the wireless power transfer subsystem that defines an operating volume of 20 cm × 25 cm × 15 cm in which the measuring devices can be correctly supplied with no need for batteries. This subsystem is implemented using the inductive coupling of *LC* resonant circuits.

In Sections II-A and II-B, the measuring device and the WPT subsystem are described in detail.

A. Measuring Device

Fig. 2 reports the block diagram of the measuring device. The core of the unit is an ATmega328P microcontroller; this device controls and supervises all the operations needed for the measuring process (peripheral diagnostics, sensors reading, and wireless transmitting). The microcontroller is chosen for its low-power capabilities (picoPower technology from Atmel, San Jose, CA, USA), programming simplicity and documentation availability. Most of the on-board peripherals

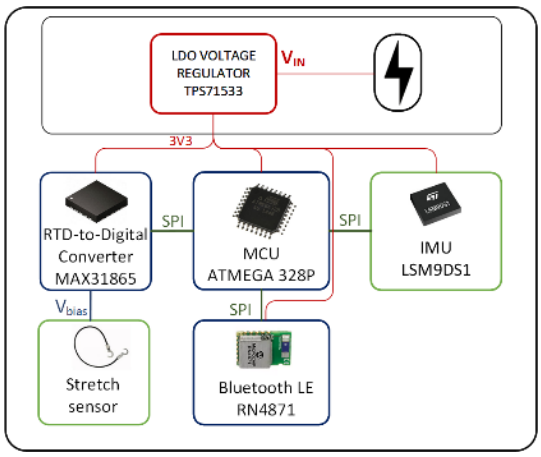

Fig. 2. Block diagram of the measuring device.

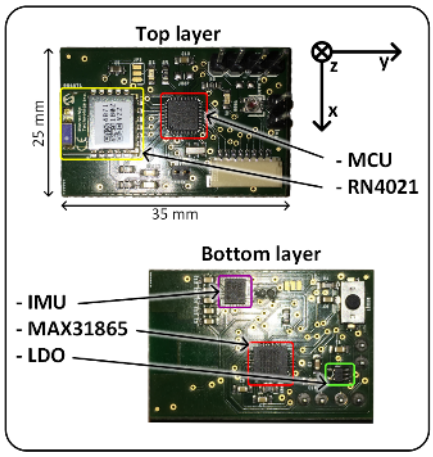

Fig. 3. Representation of the fabricated PCB with the main components highlighted and IMU axes orientation.

can be selectively turned OFF when not in use to reduce the overall power consumption. The chosen package is the smallest available (ML-32 pin, 5 mm × 5 mm).

The 3-D orientation of the board is retrieved through an IMU (LSM9DS1, produced by STMicroelectronics, Geneva, Switzerland), which includes accelerometer, gyroscope, and magnetometer, small form factors and good power-saving features make it suitable for this application [27]. Since the PCB board is bound to the first phalanx, the IMU is used to measure the finger position and orientation. The angle between the first and the second phalanx is measured by a stretch sensor (from Image SI, Inc., Staten Island, NY, USA), made by a conductive rubber that varies its resistance depending on the stress to which it is subjected. To couple this filament with the dorsal part of the finger, a pair of fabric rings were produced. The length of the stretch sensor can be chosen according to the specific length of the phalanges. The filament has a nominal resistance, in the absence of stress, of about 395 Ω/cm. The stretch sensor resistance is measured by a specific integrated circuit, MAX31865 from Maxim Integrated, San Jose, CA, USA, that eases resistance measurement and offers diagnostic and power-saving features.

The wireless communication channel is provided by a BLE module, RN4871 from Microchip Technology, Chandler, AZ, USA, which guarantees low-power functionalities. The generic attribute profile (GATT) roles are used to exchange data in accordance with the BLE protocol [28]; on the server side (measuring device), four custom characteristics are defined to store sensors data from IMU and stretch sensor. At each measuring cycle, the microcontroller updates the data in the characteristics. After a Bluetooth connection between the two modules is established, on the client side (computer program), a subscription to the cited characteristics is done and the notification function is activated. Every time the microcontroller updates the data on the server side, they are automatically transferred to the client module. The update rate of the measuring device is 30 Hz. The data transmission lasts about 1.7 ms, and then, the module reads the sensors for the following 31.1 ms. The board can be supplied directly with a stable voltage of 3.3 V or with an unregulated voltage from 3.45 to 24 V thanks to an on-board low-dropout (LDO) voltage regulator (TPS71533, Texas Instruments, Dallas, TX, USA). The average power consumption of the measuring device is 67.72 mW. In Fig. 3, the top and the bottom layers of the measuring device are shown. The actual size of the board is 25 mm × 35 mm.

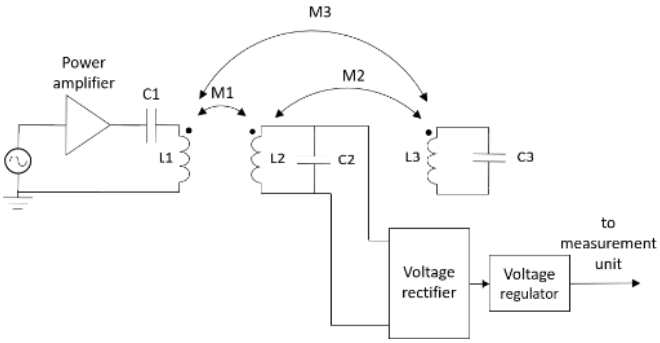

Fig. 4. Architecture of the WPT subsystem, where a relay resonator (L_3 and C_3) is placed above the primary resonator (L_1 and C_1) and tuned to the same resonant frequency.

B. WPT Subsystem

The architecture of the developed WPT subsystem is shown in Fig. 4. The core of this subsystem is comprised of two mutually coupled inductors, i.e., L_1 and L_2. The custom-made transmitter coil L_1 is comprised of 15 turns of enameled copper wire, which is wound around a 25 cm × 20 cm wooden rectangular support. The receiver coil, L_2, to be worn on the back of the hand, is a cylindrical coil wrapped around a ferrite core with a diameter of 11 mm. The transmitter and receiver coils are connected to lumped capacitors to implement a series and parallel resonator, respectively. Furthermore, L_3 and C_3 constitute a relay resonator of the same nominal size as the primary resonator and weakly coupled with it. The relay resonator strengthens the magnetic field in the operational volume above the primary resonator and, at the same time, produces a more uniform field amplitude distribution. Therefore, it improves the performance with respect to the

single-resonator configuration presented in [26], which was comprised only of the transmitter and receiver resonators. All three resonators are tuned to the same resonance frequency of 108 kHz.

The transmitter resonator is driven by a sinusoidal signal at the resonant frequency, buffered by a power amplifier based on the OPA541 operational amplifier connected in the voltage-follower configuration. The OPA541 was chosen due to its monolithic construction and its capability of delivering high currents up to 5 A. The receiver resonator is connected to a diode bridge rectifier circuit that converts the sinusoidal signal to a dc level. The voltage at the output of the rectifier is clipped to 13 V using a Zener diode, to avoid damaging the downstream circuits. Then, a voltage regulator provides the required voltage of 3.3 V to the measuring device.

III. Experimental Tests

In this section, the setup and results of experimental tests are presented. First, the finger tracking system is characterized in a standalone fashion. Then, the gesture recognition method is evaluated. Finally, simulations and experiments related to the WPT subsystem and its integration with the measurement section are presented.

A. Standalone Finger Tracking System

A series of tests were performed on the measuring system to evaluate the overall functionalities. The first test is aimed at evaluating the behavior of the sensors with which the system is equipped. In the first test, the IMU has been used as an inclinometer to retrieve the pitch angle and roll angle, starting from the acceleration measured on the three axes. The values of the angles are obtained through the following equations [(1) and (2)] according to the rotation sequence $\mathbf{R}_{yxz}$ [29], the frame of reference and G_x, G_y, and G_z symbols are described in Figs. 1 and 3

$$\theta = \text{atan}\left(\frac{G_y}{\sqrt{G_x^2 + G_z^2}}\right) \tag{1}$$

$$\Phi = \left(\frac{-G_x}{G_z}\right). \tag{2}$$

The device has been bounded to a mechanical structure by which a known angle can be imposed. The comparison between the data retrieved from the accelerometer and the imposed known angle are arranged in Fig. 5. The calculated coefficients of determination (R^2) are, respectively, 0.9985 and 0.9996 for the roll and pitch angles.

The second test performed is a characterization of the stretch sensor. The setup includes a digital multimeter HP34401A to evaluate the sensor resistance and an ARAMIS optical system (by GOM, Braunschweig, Germany) that performs digital image correlation. This device recognizes a specific pattern on the tracked object surface and calculates the reciprocal distances between the points. When the sensor is stretched, the ARAMIS system can calculate the overall lengthening. As it is reported in Fig. 6, the sensor is characterized by good linearity in the strain interval 0%–10%, the calculated gauge factor is 4.73.

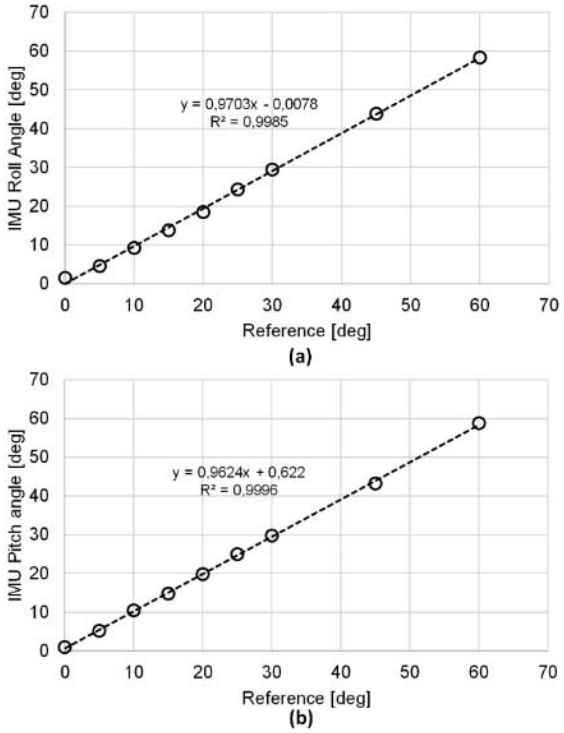

Fig. 5. Measured inclination in terms of the reference for (a) roll and (b) pitch angles.

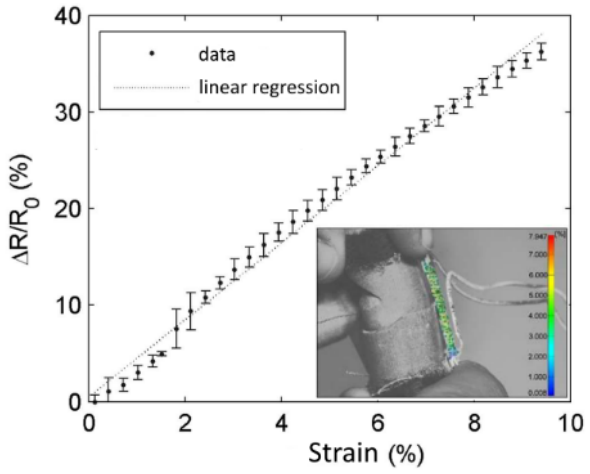

Fig. 6. Stretch sensor characterization in the strain interval 0%–10% ($R_0 = 300\ \Omega$). The detail shows the ARAMIS GOM output.

B. Gesture Recognition: Method and Experimental Results

We perform a test to examine the hand gesture recognition capability of our wearable device. The method for recognizing the gestures is based on measurement results obtained by the stretch sensor and the accelerometer. First, we define a limited set of hand poses that the system must recognize. In Fig. 7(a), the chosen poses are shown. The first one (*1*) is used as a starting point from which the movements are executed. The three gestures are indicated as G1 (from position 1 to 2), G2 (from 1 to 3), and G3 (from 1 to 4). All the movements described can be performed with the hand palm upward or downward defining four other

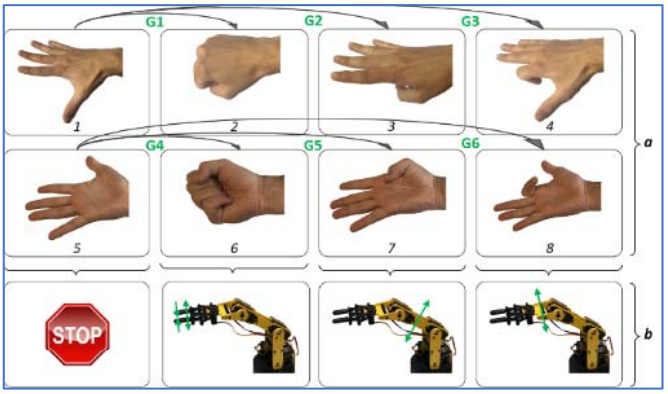

Fig. 7. (a) Gestures and poses description. (b) Lynx robotic arm axis movements.

poses (5–8) and three more gestures (G4–G6). The system is then interfaced with a Lynx 6 robotic arm [30] (from Lynxmotion, Inc., Swanton, VT, USA), a didactic five-axis robotic arm moved by servo motors. The entire robot is driven by an SSC-32 board (Lynxmotion) that provides an easy-to-use serial interface to control the motors. In Fig. 7(b), the green arrows describe arm movements associated with the gestures: G1 and G4 permit to open or close the robot gripper, G2 and G5 move the second axis, and G3 and G5 move the third one.

The device is worn by a male subject on the index and thumb fingers of the right hand, and every movement is performed multiple times. To recognize the hand poses, we analyze two main data sources. The finger flection is obtained by observing the stretch sensors resistance variation. The hand orientation is retrieved from the accelerometer of the on-board IMU. In this case, we can turn OFF the magnetometer and the gyroscope to reduce the overall power consumption. According to the technical document [27], the gyroscope is the most power-consuming peripheral, and it requires 4 mA of supply current in normal mode; the accelerometer and magnetic sensor in normal mode have a current consumption of about 600 μA in total. The average power required by the wearable device is reduced to 54.52 mW.

In Fig. 8(a) and (b), an excerpt of the data measured by the system during the execution of the gestures G1 and G3 is shown. The two tracks, in each figure, show the resistance values of the stretch sensors. This reflects the flexion of the thumb and index when the movement is performed, and the resistance increases when the sensor is stretched (during the flexion movement) and decreases when released (finger extension). In G1 gesture execution, both fingers are flexed [Fig. 8(a)], while in G3 [Fig. 8(b)], thumb remains extended. It is possible to notice a considerable spike before the releasing phase. This behavior is expected as characteristic of the material by which the sensor is composed [31]. Even if the spike amplitude is comparable to the total range of the signal, it runs out very quickly. All signals are then processed by applying a moving average to smooth the unnecessary fast transitions. In this case, a window of 30 samples is used. However, different window lengths could be used, depending on the specific conditions and on the application.

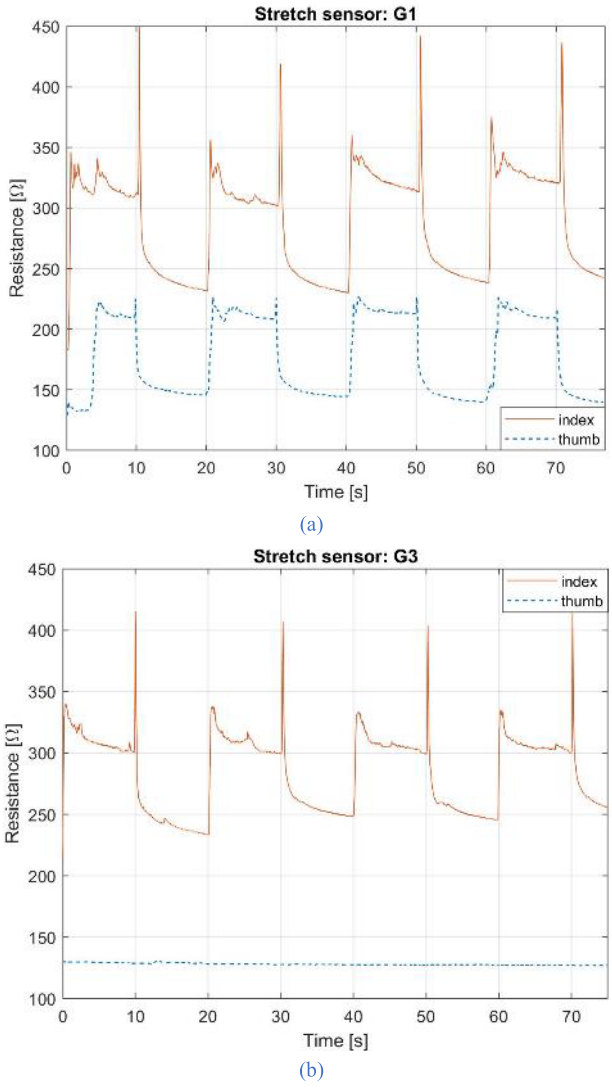

Fig. 8. Raw data of stretch sensor resistance variation (index: red solid line and thumb: blue dashed line). During the execution of: (a) G1 gesture and (b) G3 gesture.

Another aspect to consider is the sensor characteristic recovery time due to the material relaxation. This has to be assessed in order to discriminate if the finger is flexed or not correctly. Data analysis was performed to determine if the eight poses can be univocally distinguished and to establish the thresholds to implement an automatic recognition algorithm. We divide the range in which it is reasonable to expect the resistance values in 30 subintervals and count the number of samples that fall within each of these. In Fig. 9, the histogram of the resistance related to the three gestures performed with the hand palm downward is shown. In the first one (G1), the movement is characterized by the flexion of both fingers; we can observe the presence of two peaks for each finger. The thumb presents the first peak in the interval (145.8–150) Ω where about 16% of the samples fall; the second maximum is in the interval (187.5–191.7) Ω with a value of 10%. Considering a confidence interval of about 40%, the two sets are sufficiently disjoint to distinguish the two poses uniquely. These considerations can be repeated in a similar way for the index stretch

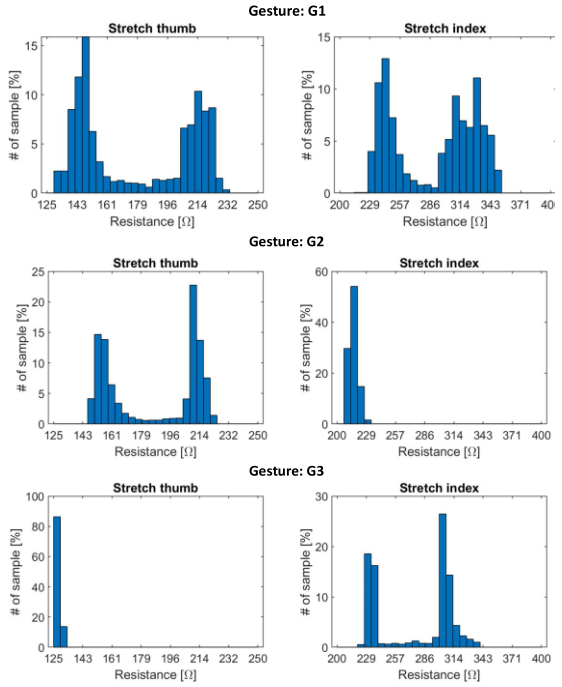

Fig. 9. Frequency distribution of the stretch sensor values for downward hand palm gestures.

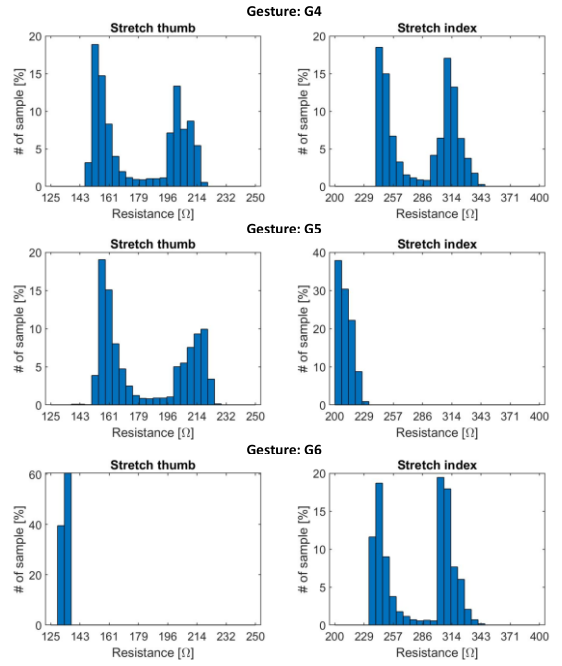

Fig. 10. Frequency distribution of the stretch sensor values for upward hand palm gestures.

sensors. Continuing the analysis for the G2 gesture, we have a single-finger flexion, the thumb, while the index remains extended. This is reflected in the data analysis results where the thumb has two maxima (flexed and extended positions); the index graph has the 85% of the values concentrated in the interval (206.7–220) Ω.

In Fig. 10, the data analysis of the gestures G4–G6 performed with the palm upward is shown. The initial resistance

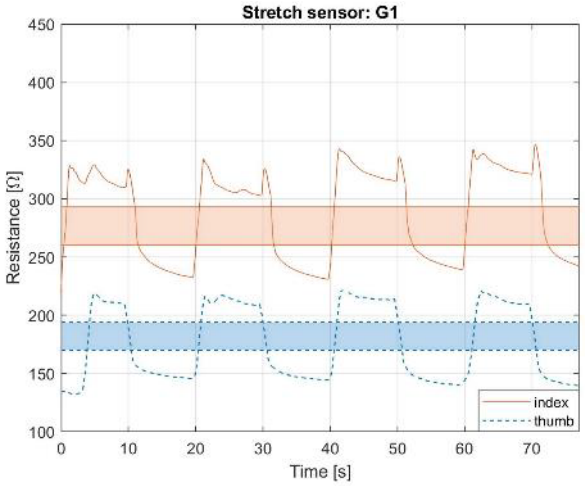

Fig. 11. Filtered data of stretch sensor resistance variation during the execution of G1 gesture with recognition thresholds (index: red and thumb: blue).

value depends, among other factors, especially on how the device is worn. To avoid any ambiguity, it is good practice to perform a quick calibration before each use by repeatedly flexing and extending the monitored fingers. This permits to define two thresholds: one above which the finger is considered flexed and another one below which it is considered fully extended. In the reported analysis, these thresholds are: thumb extended—1708 Ω, thumb flexed: 1958 Ω, index extended: 260 Ω, and index flexed: 2933 Ω. The reported analysis, performed on the filtered data, is visible in Fig. 11, where the thresholds are shown with the respective colors (blue for the thumb and red for index). When a sample falls above or below the shaded area, it is recognized as flexed or extended.

As mentioned earlier, to differentiate between the upward and downward palm gestures group, the acceleration along the z-axis is considered. In Table I, the z-axis acceleration data are listed for different gestures. In this case, we analyze the maximum and minimum value of each try. In the first group (G1–G3, hand palm downward), the values are always negative, even when the gestures are performed. Symmetrically, in the second group (G4–G6), the values are positive. With this further parameter, we can distinguish between every pose defined in the set.

C. Wireless Power Transfer Tests

Further tests have been carried out to verify the compatibility between the WPT system and the measurement system. In these tests, the measurement system and the WPT system were tested jointly. Specifically, the measurement board was connected directly to the 3.3-V output of the WPT system, bypassing the onboard LDO voltage regulator. The WPT system was turned ON with a voltage supply of the power amplifier of $V_{DC} = \pm 12$ V, a zero-mean sinusoidal input signal with frequency $f = 108.7$ kHz, generating an rms current of 1.24 A in the transmitting coil. The relay coil was placed above the transmitting coil at a 15-cm distance, supported by wooden stands. The receiving resonator was connected to the

TABLE I

MAXIMUM AND MINIMUM z-AXIS ACCELERATION VALUES RECORDED DURING GESTURES EXECUTION

G #	Z acceleration [g]			
	thumb		index	
	min	max	min	max
1	-0.96	-0.44	-1.16	-0.70
2	-0.94	-0.28	-1.13	-0.73
3	-0.84	-0.41	-1.30	-0.73
4	0.14	0.64	0.39	1.08
5	0.13	0.70	0.78	1.23
6	0.40	0.65	0.60	1.09

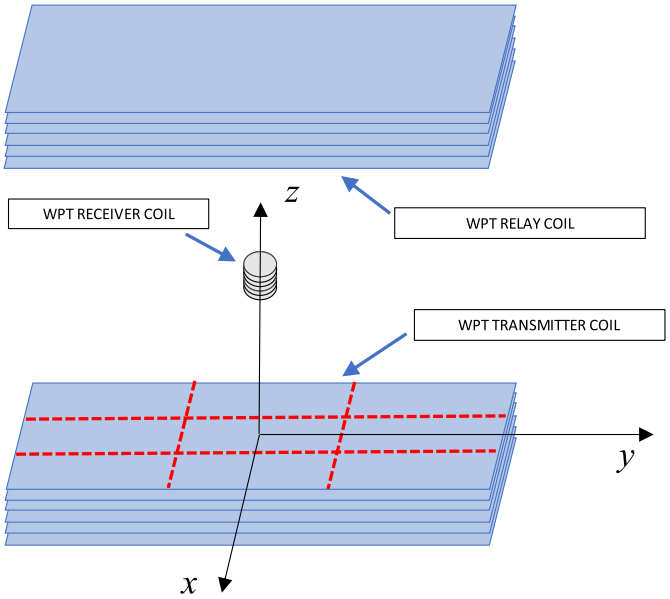

Fig. 12. Setup of the WPT performance test. The red dashed lines denote the nine areas in which the surface of the transmitting coil has been divided.

rectifier and regulator, and the output of the regulator was connected to the two measuring devices.

The test aimed to verify that the WPT system was able to supply the measuring system throughout the considered operational volume. Another aim of this test is to compare the performance with that achieved in the single-resonator configuration. Such configuration, which is described in [26], is the same as that used in this article, except for the absence of the relay coil, resulting in a less homogeneous field.

To test the performance of the WPT system, the transmitter surface was ideally divided into nine areas and the output voltage of the rectifier (before the voltage regulator) was measured at different vertical distances, keeping the receiver coil in the vertical orientation. Therefore, a 3-D grid of measurement positions was defined within the operational volume. The test setup is shown by the diagram in Fig. 12.

This setup confirmed that the two measuring devices were correctly powered, able to acquire and transmit data. The results, as shown in Fig. 13, prove that the system is operational throughout the considered volume of size

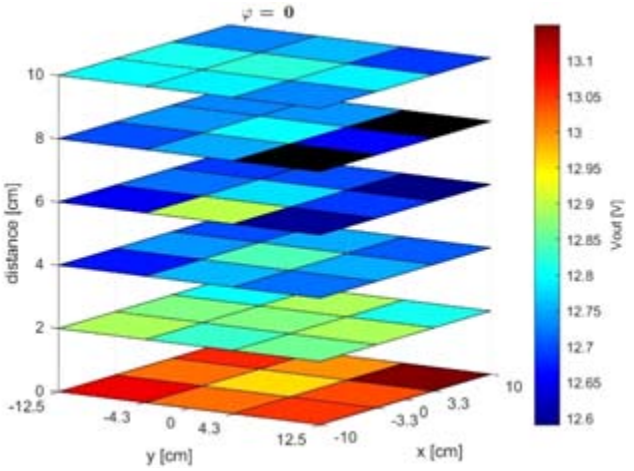

Fig. 13. Experimental results. Output voltage of the rectifier in the WPT circuit at several positions above the transmitting coil.

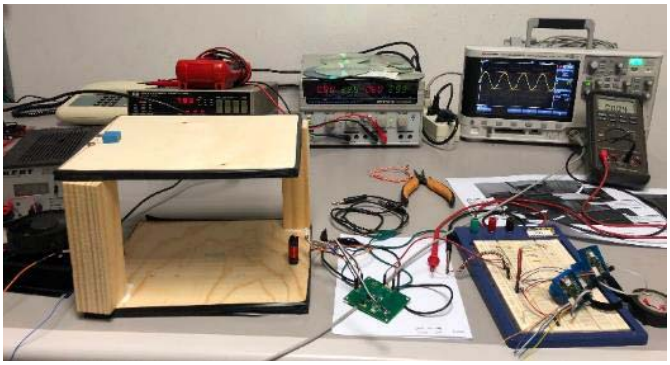

(a)

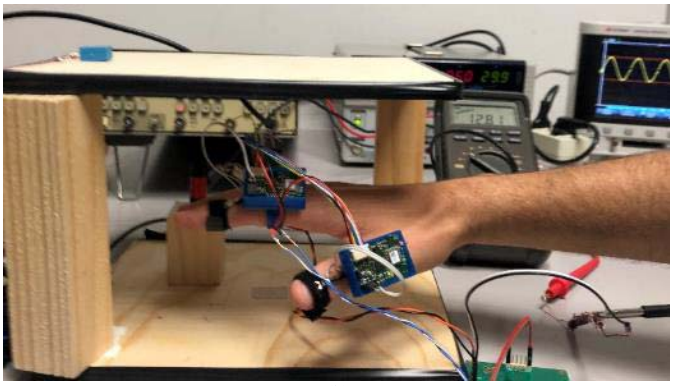

(b)

Fig. 14. (a) Photograph of the experimental setup used to validate the operation of the relay resonator configuration of the WPT subsystem. The transmitting coil and relay coil are shown on the left-hand side of the picture, where the transmitting coil is placed on the table, and the relay coil is above it on the two wooden supports; the two measuring devices are shown on the right-hand side. (b) Detail of the two measuring devices worn on the index finger and thumb inside the operating range of the WPT apparatus.

25 cm × 20 cm × 15 cm. The voltage measured at the output of the rectifier is between 12.6 and 13.2 V. Thus, a range of variation of approximately 0.6 V is observed using the relay coil, smaller than the 20-V range of variation observed in the single-resonator configuration [26]. Furthermore, using a single resonator, the maximum operating distance is 8 cm,

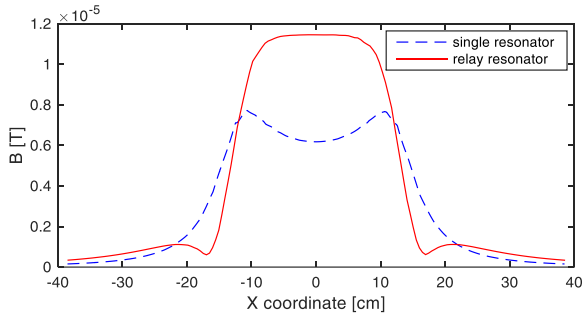

Fig. 15. Simulated B field values at 4-cm height above the transmitting coil, along the x-axis direction, in the single-resonator and relay resonator configurations. The transmitting coil is placed in the xy plane.

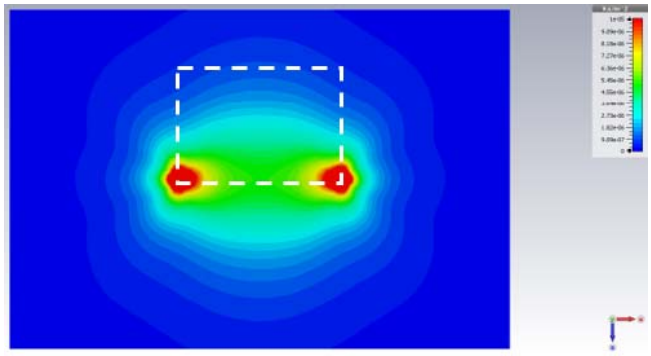

Fig. 16. Simulated B field in the xz plane in the single-resonator configuration. The white dashed line denotes the operating volume of the WPT system. The transmitting coil is placed in the xy plane.

and thus, the system is not operational in the upper portion of the considered volume due to the inhomogeneous nature of the magnetic field. This problem is solved by the relay coil configuration. A picture of the test setup comprised of the measurement system powered by the WPT system is shown in Fig. 14.

To compare the field distribution in the two considered geometrical configurations, i.e., the single resonator and the relay resonator, a simplified model was modeled and simulated by a full-wave environment [32] adopting the finite-element method numerical simulator. The transmitting coil was modeled as a single-current loop with the profile of the real one with an rms current of 1 A. The simulation results in the two geometrical configurations are shown in Fig. 15–17. It is possible to notice that, assuming the same rms current of 1 A in the transmitting coil, the relay resonator allows for a stronger and more homogenous field inside the operating volume. Specifically, in Fig. 15, it is shown that the field magnitude in the relay configuration is 11.5 μT at the center of the operating volume ($x = 0$, $y = 0$, and $z = 4$ cm), whereas it is 6.2 μT in the single-resonator configuration in the same position.

The results of the simulation were compared with the International Commission on Non-Ionizing Radiation Protection (ICNIRP) limits for the safe exposure of the public and workers [33]. By considering that the number of turns of the transmitting and relay coils is 15 and that the current in the transmitting coil is 1.24 A, we have observed that the emitted

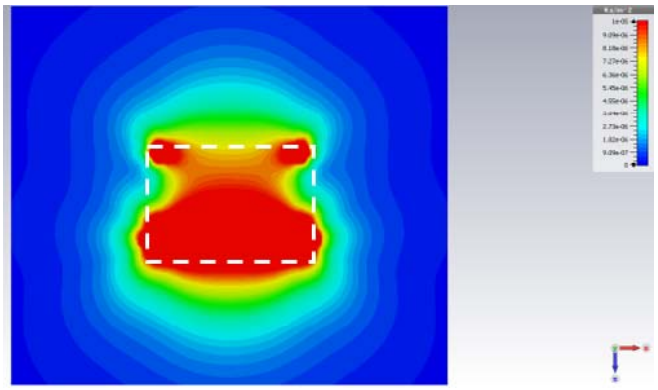

Fig. 17. Simulated B field in the relay resonator configuration. The dashed white line denotes the operating volume of the WPT system. The transmitting coil is placed in the xy plane, whereas the relay resonating coil is placed above it, parallel to the xy plane, at 15-cm distance.

field B in the relay configuration is 213 μT. This exceeds the ICNIRP exposure limit for workers in the frequency range 3 kHz to 10 MHz, which is 100 μT, approximately doubling it. This is mainly due to the increased power requested from the electronics and to the geometry of the three coils, which is not optimized. The mitigation of the B field emission can be obtained, depending on the load, by controlling the resonant current once a proper coil geometry is designed.

IV. Conclusion

A wearable and wirelessly powered system for tracking finger motion and recognizing hand gestures was presented. The system architecture is based on two measuring devices, worn on the thumb and index fingers, and a wireless power transfer subsystem. Experimental tests performed on a prototype show that the developed system tracks the extension and flexion of two fingers and transmits data via Bluetooth with an update rate of 30 Hz. Furthermore, based on the acquired stretch-sensor and accelerometer data, the system may be able to detect six predefined hand gestures, which may be used to control a robotic arm. In this preliminary study, data analysis allowed the validation of obtained results and confirmed the feasibility of gesture recognition. The development and characterization of gesture recognition algorithms will be the subject of future developments. The wireless power transfer subsystem can supply 110 mW to the measurement section within an operating volume of 25 cm $\times$ 20 cm $\times$ 15 cm, which is suitable for several short-range finger tracking, gesture recognition, and telemanipulation scenarios. Future work includes development and engineering activities aimed at improving the realized prototype, reducing its physical dimensions and current consumption. These activities will also enable tests on multiple subjects.

References

[1] F. Gonzalez, F. Gosselin, and W. Bachta, "A 2-D infrared instrumentation for close-range finger position sensing," *IEEE Trans. Instrum. Meas.*, vol. 64, no. 10, pp. 2708–2719, Oct. 2015.

[2] D. De Carli *et al.*, "Measuring intent in human-robot cooperative manipulation," in *Proc. IEEE Int. Workshop Haptic Audio Vis. Environ. Games*, Nov. 2009, pp. 159–163.

[3] M. Zabri Abu Bakar, R. Samad, D. Pebrianti, M. Mustafa, and N. R. H. Abdullah, "Computer vision-based hand deviation exercise for rehabilitation," in *Proc. IEEE Int. Conf. Control Syst., Comput. Eng. (ICCSCE)*, Nov. 2015, pp. 389–394.
[4] T. Koivukangas and J. P. A. Katisko, "On the comparison of the accuracies of optical tracking and EMTS modalities of surgical navigators," in *Proc. 5th Cairo Int. Biomed. Eng. Conf.*, Dec. 2010, pp. 29–32.
[5] V. Pasku *et al.*, "Magnetic field-based positioning systems," *IEEE Commun. Surveys Tuts.*, vol. 19, no. 3, pp. 2003–2017, 3rd Quart., 2017.
[6] A. H. Moreira, S. Queiros, J. Fonseca, P. L. Rodrigues, N. F. Rodrigues, and J. L. Vilaca, "Real-time hand tracking for rehabilitation and character animation," in *Proc. IEEE 3nd Int. Conf. Serious Games Appl. Health (SeGAH)*, May 2014, pp. 1–8.
[7] A. R. Várkonyi-Kóczy and B. Tusor, "Human–computer interaction for smart environment applications using fuzzy hand posture and gesture models," *IEEE Trans. Instrum. Meas.*, vol. 60, no. 5, pp. 1505–1514, May 2011.
[8] Z. Xiao, W. Hu, C. Liu, H. Yu, and C. Li, "Noncontact human–machine interface with planar probing coils in a differential sensing architecture," *IEEE Trans. Instrum. Meas.*, vol. 67, no. 4, pp. 956–964, Apr. 2018.
[9] J. Hugle, J. Lambrecht, and J. Kruger, "An integrated approach for industrial robot control and programming combining haptic and non-haptic gestures," in *Proc. 26th IEEE Int. Symp. Robot Hum. Interact. Commun. (RO-MAN)*, Aug. 2017, pp. 851–857.
[10] A. Asokan, A. Pothen, and R. Vijayaraj, "ARMatron—A wearable gesture recognition glove: For control of robotic devices in disaster management and human Rehabilitation," in *Proc. Int. Conf. Robot. Automat. Humanitarian Appl. (RAHA)*, Dec. 2016, pp. 1–5.
[11] P. K. Pisharady and M. Saerbeck, "Recent methods and databases in vision-based hand gesture recognition: A review," *Comput. Vis. Image Understand.*, vol. 141, pp. 152–165, Dec. 2015.
[12] S. Yang, P. Premaratne, and P. Vial, "Hand gesture recognition: An overview," in *Proc. 5th IEEE Int. Conf. Broadband Netw. Multimedia Technol.*, Nov. 2013, pp. 63–69.
[13] A. El-Sawah, N. Georganas, and E. Petriu, "A prototype for 3-D hand tracking and posture estimation," *IEEE Trans. Instrum. Meas.*, vol. 57, no. 8, pp. 1627–1636, Aug. 2008.
[14] N. H. Dardas and N. D. Georganas, "Real-time hand gesture detection and recognition using bag-of-features and support vector machine techniques," *IEEE Trans. Instrum. Meas.*, vol. 60, no. 11, pp. 3592–3607, Nov. 2011.
[15] F. Santoni, A. De Angelis, I. Skog, A. Moschitta, and P. Carbone, "Calibration and characterization of a magnetic positioning system using a robotic arm," *IEEE Trans. Instrum. Meas.*, vol. 68, no. 5, pp. 1494–1502, May 2019.
[16] V. Pasku, A. De Angelis, M. Dionigi, A. Moschitta, G. De Angelis, and P. Carbone, "Analysis of nonideal effects and performance in magnetic positioning systems," *IEEE Trans. Instrum. Meas.*, vol. 65, no. 12, pp. 2816–2827, Dec. 2016.
[17] L.-H. Jhang, C. Santiago, and C.-S. Chiu, "Multi-sensor based glove control of an industrial mobile robot arm," in *Proc. Int. Autom. Control Conf. (CACS)*, Nov. 2017, pp. 1–6.
[18] M. Borghetti, E. Sardini, and M. Serpelloni, "Sensorized glove for measuring hand finger flexion for rehabilitation purposes," *IEEE Trans. Instrum. Meas.*, vol. 62, no. 12, pp. 3308–3314, Dec. 2013.
[19] P.-C. Hsiao, S.-Y. Yang, B.-S. Lin, I.-J. Lee, and W. Chou, "Data glove embedded with 9-axis IMU and force sensing sensors for evaluation of hand function," in *Proc. 37th Annu. Int. Conf. IEEE Eng. Med. Biol. Soc. (EMBC)*, Aug. 2015, pp. 4631–4634.
[20] Shen, "A soft stretchable bending sensor and data glove applications," *Robot. Biomimetics*, vol. 3, no. 1, 2016.
[21] B. Fang, F. Sun, H. Liu, and C. Liu, "3D human gesture capturing and recognition by the IMMU-based data glove," *Neurocomputing*, vol. 277, pp. 198–207, Feb. 2018.
[22] Z. Zhang, H. Pang, A. Georgiadis, and C. Cecati, "Wireless power transfer—An overview," *IEEE Trans. Ind. Electron.*, vol. 66, no. 2, pp. 1044–1058, Feb. 2019.
[23] A. Kurs, A. Karalis, R. Moffatt, J. D. Joannopoulos, P. Fisher, and M. Soljacic, "Wireless power transfer via strongly coupled magnetic resonances," *Science*, vol. 317, no. 5834, pp. 83–86, Jul. 2007.
[24] V. J. Brusamarello, Y. B. Blauth, R. de Azambuja, I. Müller, and F. R. de Sousa, "Power transfer with an inductive link and wireless tuning," *IEEE Trans. Instrum. Meas.*, vol. 62, no. 5, pp. 924–931, May 2013.
[25] A. De Angelis, M. Dionigi, P. Carbone, and M. Mongiardo, "Characterization and performance measurements of mid-range wireless power transfer links," in *Proc. IEEE Int. Instrum. Meas. Technol. Conf.*, May 2016, pp. 1–5.
[26] P. Bellitti *et al.*, "Development of a wirelessly-powered wearable system for finger tracking," in *Proc. IEEE Int. Instrum. Meas. Technol. Conf. (I2MTC)*, May 2019, pp. 1–5.
[27] *iNEMO Inertial Module: 3D Accelerometer, 3D Gyroscope, 3D Magnetometer*, LSM9DS1 datasheet, STMicroelectronics, Geneva, Switzerland, Mar. 2015.
[28] R. Heydon, *Bluetooth Low Energy: The Developer's Handbook*. Upper Saddle River, NJ, USA: Prentice-Hall, 2014.
[29] M. Pedley, *Tilt Sensing Using a Three-Axis Accelerometer, AN3461 Rev. 6*, Freescale Semiconductor, Austin, TX, USA, Mar. 2013.
[30] *Lynx 6—L6AC-KT Manual*, Lynxmotion, Swanton, VT, USA, 2019.
[31] Images Scientific Instruments Inc. *Flexible Stretch Sensors*. Accessed: Feb. 1, 2020. [Online]. Available: http://www.imagesco.com/sensors/stretch.pdf
[32] *CST Microwave Studio*. Accessed: Feb. 1, 2020. [Online]. Available: htpps://www.cst.com
[33] International Commission on Non Ionizing Radiation Protection, "Guideline for limiting exposure to time-varing electric and magnetic fields (1 Hz to 100 kHz)," *Health Phys.*, vol. 99, no. 6, pp. 818–836, Dec. 2010.

Paolo Bellitti was born in Brescia, Italy, in 1990. He received the B.Sc. and M.Sc. degrees from the University of Brescia, Brescia, and the Ph.D. degree in technology for health from the Department of Information Engineering, University of Brescia, in 2019.

In 2016, he received a research grant from the Department of Information Engineering, University of Brescia, to work on measurement systems in biomedical field. He was a Visiting Ph.D. Student with the Universitat Politècnica de Catalunya in 2018. He is currently a Post-Doctoral Fellow with the University of Brescia. His research interests are in the fields of industrial and biomedical measurement devices.

Alessio De Angelis (Member, IEEE) received the Ph.D. degree in information engineering from the University of Perugia, Perugia, Italy, in 2009.

From 2010 to 2013, he was a Researcher with the Signal Processing Laboratory, KTH Royal Institute of Technology, Stockholm, Sweden. Since 2013, he has been with the Department of Engineering, University of Perugia, where he became an Associate Professor in 2018. His research interests include instrumentation and measurement, positioning systems (using a magnetic field and ultrasound), statistical signal processing, system identification, and sensors.

Dr. De Angelis has been serving as an Associate Editor for IEEE TRANSACTIONS ON INSTRUMENTATION AND MEASUREMENT since 2019.

Marco Dionigi is currently an Assistant Professor with the Department of Engineering, University of Perugia, Perugia, Italy. His current research interests are in the fields of microwave and millimeter-wave waveguide component modeling and optimization, wireless power transfer systems modeling and design, and microwave sensor modeling and design.

Emilio Sardini received the M.Sc. degree in electronics engineering from the Politecnico di Milano, Milan, Italy, in 1983.

He is currently the Coordinator of the Technology for Health Ph.D. Program and the Director of the Department of Information Engineering, University of Brescia, Brescia, Italy. He is also a member of the Academic Senate, Board of Directors, University of Brescia, and the Deputy Dean of the Engineering Faculty. His research focuses on electronic instrumentation, sensors and signal conditioning electronics, and the development of autonomous sensors for biomedical applications.

Mauro Serpelloni received the Laurea (*cum laude*) and the Ph.D. degrees in electronic instrumentation from the University of Brescia, Brescia, Italy, in 2003 and 2006, respectively.

Since 2010, he has been an Associate Professor with the Department of Information Engineering, University of Brescia, where he is involved in teaching sensors, electronic instrumentation, sensors for biosignals, and mechatronics. He is currently the Manager of a new laboratory for aerosol jet printing. His research interests include electronic instrumentation, sensors, contactless transmissions between sensors and electronics, and signal processing for microelectromechanical systems.

Antonio Moschitta (Member, IEEE) received the Ph.D. degree from the University of Perugia, Perugia, Italy, in 2002.

He is currently an Associate Professor with the University of Perugia. His research interests include power quality, A/D, D/A time-to-digital conversion, indoor positioning, and estimation theory. He has authored or coauthored more than 120 articles.

Dr. Moschitta was the General Co-Chair of the 2012 IEEE Workshop on Environmental, Energy, and Structural Monitoring Systems 2012. He is currently the Chair of the IEEE Systems Council Italian Chapter. He has appeared in several international journals or conference proceedings.

Paolo Carbone (Fellow, IEEE) received the Laurea and Ph.D. degrees from the University of Padua, Padua, Italy, in 1990 and 1994, respectively.

From 1994 to 1997, he was a Researcher with Roma Tre University, Rome, Italy. From 1997 to 2002, he was a Researcher with the University of Perugia, Perugia, Italy, where he has been a Full Professor since 2002, where he teaches courses in instrumentation and measurement and in statistical signal processing. He has been involved in various research projects sponsored by private and public funds. He has authored or coauthored more than 200 articles.

Prof. Carbone has appeared in international journals and conference proceedings. He served as an Associate Editor for the IEEE TRANSACTIONS ON CIRCUITS AND SYSTEMS—PART II from 2000 to 2002 and the IEEE TRANSACTIONS ON CIRCUITS AND SYSTEMS—PART I from 2005 to 2007. He was the President of the IEEE Systems Council from 2016 to 2017.